Genome-wide Screening Identifies SFMBT1 as an Oncogenic Driver in Cancer with VHL Loss

Xijuan Liu,[1] Jeremy M. Simon,[1,2,3] Haibiao Xie,[4] Lianxin Hu,[1,9] Jun Wang,[1] Giada Zurlo,[1,9] Cheng Fan,[1] Travis S. Ptacek,[1,3] Laura Herring,[5,6] Xianming Tan,[1] Mingjie Li,[1,9] Albert S. Baldwin,[1] William Y. Kim,[1] Tao Wu,[7] Marc W. Kirschner,[7] Kan Gong,[4] and Qing Zhang[1,8,9,10,*]

[1]Lineberger Comprehensive Cancer Center, University of North Carolina School of Medicine, Chapel Hill, NC 27599, USA
[2]Department of Genetics, University of North Carolina, Chapel Hill, NC 27599, USA
[3]UNC Neuroscience Center, University of North Carolina, Chapel Hill, NC 27599, USA
[4]Department of Urology, Peking University First Hospital, Beijing, China
[5]Department of Pharmacology, University of North Carolina, Chapel Hill, NC 27599, USA
[6]UNC Proteomics Core Facility, University of North Carolina, Chapel Hill, NC 27599, USA
[7]Department of Systems Biology, Harvard Medical School, Boston, MA 02115
[8]Department of Pathology and Laboratory Medicine, University of North Carolina, Chapel Hill, NC 27599, USA
[9]Department of Pathology, UT Southwestern Medical Center, Dallas, TX 75390, USA
[10]Lead Contact
*Correspondence: Qing.Zhang@UTSouthwestern.edu
https://doi.org/10.1016/j.molcel.2020.01.009

SUMMARY

von Hippel-Lindau (*VHL*) is a critical tumor suppressor in clear cell renal cell carcinomas (ccRCCs). It is important to identify additional therapeutic targets in ccRCC downstream of *VHL* loss besides hypoxia-inducible factor 2α (HIF2α). By performing a genome-wide screen, we identified Scm-like with four malignant brain tumor domains 1 (SFMBT1) as a candidate pVHL target. SFMBT1 was considered to be a transcriptional repressor but its role in cancer remains unclear. ccRCC patients with *VHL* loss-of-function mutations displayed elevated SFMBT1 protein levels. SFMBT1 hydroxylation on Proline residue 651 by EglN1 mediated its ubiquitination and degradation governed by pVHL. Depletion of SFMBT1 abolished ccRCC cell proliferation *in vitro* and inhibited orthotopic tumor growth *in vivo*. Integrated analyses of ChIP-seq, RNA-seq, and patient prognosis identified sphingosine kinase 1 (*SPHK1*) as a key SFMBT1 target gene contributing to its oncogenic phenotype. Therefore, the pVHL-SFMBT1-SPHK1 axis serves as a potential therapeutic avenue for ccRCC.

INTRODUCTION

The incidence of renal cancers, including renal cell and renal pelvis types, has been increasing for several decades, but the reasons for this trend are unclear (Godwin et al., 2014). Some patients at risk for clear cell renal cell carcinoma (ccRCC) carry a germline mutation in the von Hippel-Lindau (*VHL*) tumor suppressor gene, an E3 ubiquitin ligase (Kaelin, 2002). Inactivating *VHL* mutations play major roles in sporadic RCC (Haase, 2005), and loss of *VHL* accounts for up to 85% of renal cancers that are classically resistant to cytotoxic chemotherapy (Kaelin, 2002; Cancer Genome Atlas Research Network, 2013).

pVHL, the protein encoded by *VHL*, ubiquitinates hypoxia-inducible factor α (HIFα, including HIF1α and HIF2α) to mark it for degradation (Ivan et al., 2001; Jaakkola et al., 2001). Loss of pVHL therefore promotes HIFα accumulation, which contributes to the transformation phenotype of renal cancer (Kondo et al., 2003; Kondo et al., 2002). Accumulation and translocation of HIFα factors into the nucleus promotes dimerization of HIFα subunits with a constitutively expressed HIFβ subunit (Semenza, 2012). This dimer transactivates genes containing hypoxia response elements in their promoters or enhancer regions. Recent reports showed that the specific HIF2α inhibitor PT2399 inhibited primary tumor growth and invasion of a subset of kidney cancers (Cho et al., 2016; Chen et al., 2016). However, a significant portion of kidney cancers remained resistant to HIF2α inhibitor treatment (Cho et al., 2016; Chen et al., 2016), highlighting the importance of identifying additional therapeutic vulnerabilities of pVHL-deficient kidney cancer. Evidence suggests that pVHL has substrates other than HIFα (Gamper et al., 2012; Lee et al., 2015). Indeed, non-HIF substrates may account for different subtypes of *VHL* disease (type 2A and 2B versus 2C) (Clifford et al., 2001; Gordeuk et al., 2004; Hoffman et al., 2001). We recently identified ZHX2 as a new pVHL substrate that contributes to hyper-activation of NF-κB in ccRCC (Zhang et al., 2018).

To systematically identify pVHL substrates, we performed a novel genome-wide *in vitro* expression strategy coupled with a GST-binding screen for pVHL substrates and identified SFMBT1 as a direct target of pVHL. SFMBT1 was shown to be a histone reader subunit of the LSD1 demethylase complex associated with epipthelial-mesenchymal transition (Tang et al., 2013). The limited understanding of SFMBT1 has primarily focused on binding between SFMBT1 and histone tails (Zhang et al., 2013b). Additional functions for SFMBT1 and its mode of regulation, particularly in cancer, have not been explored. Here, we show

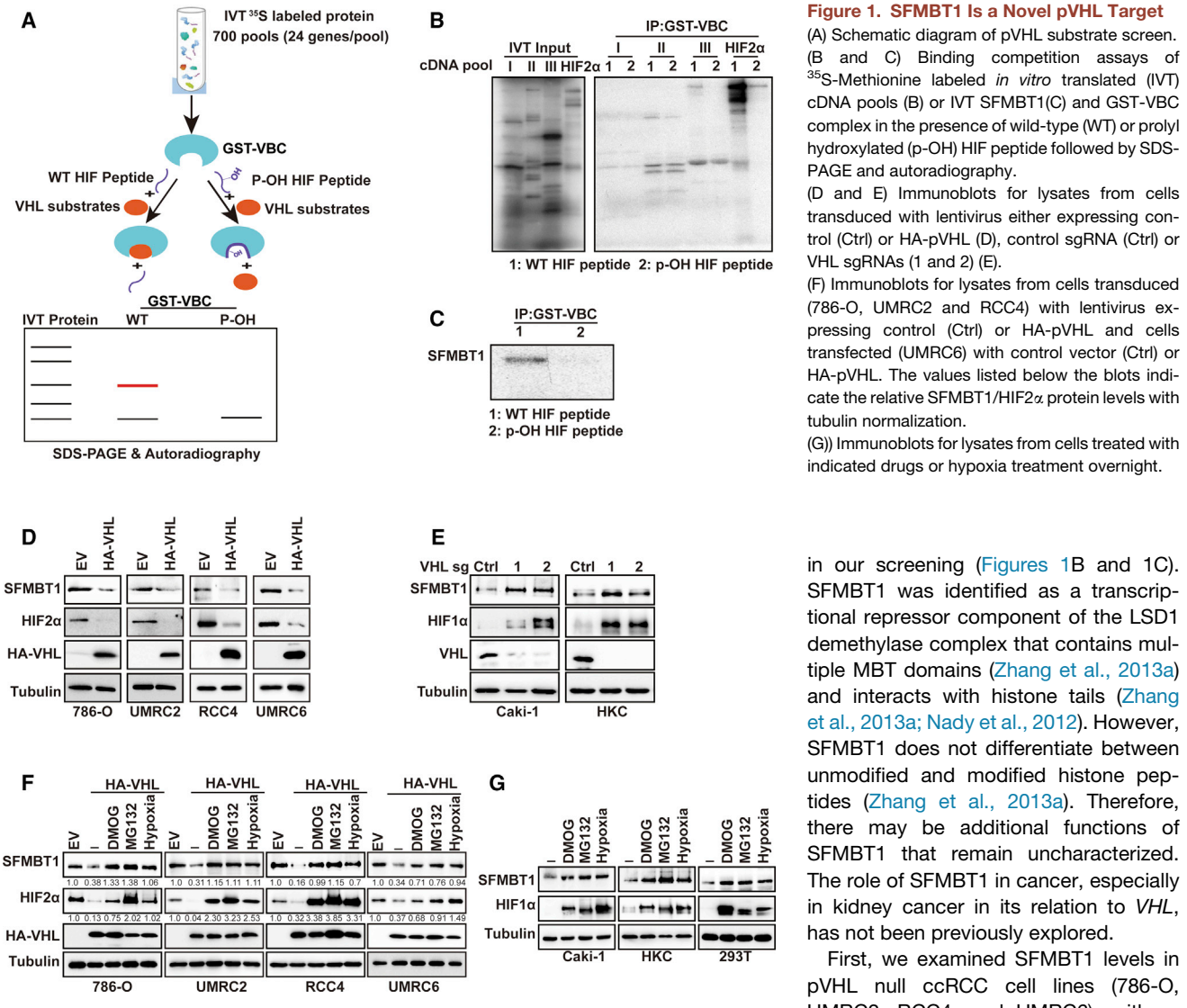

Figure 1. SFMBT1 Is a Novel pVHL Target

(A) Schematic diagram of pVHL substrate screen.

(B and C) Binding competition assays of ^{35}S-Methionine labeled *in vitro* translated (IVT) cDNA pools (B) or IVT SFMBT1(C) and GST-VBC complex in the presence of wild-type (WT) or prolyl hydroxylated (p-OH) HIF peptide followed by SDS-PAGE and autoradiography.

(D and E) Immunoblots for lysates from cells transduced with lentivirus either expressing control (Ctrl) or HA-pVHL (D), control sgRNA (Ctrl) or VHL sgRNAs (1 and 2) (E).

(F) Immunoblots for lysates from cells transduced (786-O, UMRC2 and RCC4) with lentivirus expressing control (Ctrl) or HA-pVHL and cells transfected (UMRC6) with control vector (Ctrl) or HA-pVHL. The values listed below the blots indicate the relative SFMBT1/HIF2α protein levels with tubulin normalization.

(G)) Immunoblots for lysates from cells treated with indicated drugs or hypoxia treatment overnight.

for the first time, that SFMBT1 is a target for pVHL and promotes ccRCC cell proliferation, anchorage-independent growth, as well as tumor xenograft growth. Clinically, SFMBT1 is expressed at elevated levels in renal tumors compared to adjacent normal tissue. Thus, our functional characterization of the critical SFMBT1 signaling axis in pVHL-deficient renal cancer may shed light on novel therapeutic modalities.

RESULTS

A Genome-Wide Screen Identifies SFMBT1 as a pVHL Target

Utilizing a genome-wide *in vitro* expression cloning strategy (Zhang et al., 2018), we were able to identify proteins that bind pVHL and can be competed off by the hydroxylated HIF peptide (Figure 1A). These proteins may represent potential pVHL substrates that bind to the hydrophobic substrate-binding pocket of pVHL. Here, we present evidence that Scm-like with four MBT domains 1 (SFMBT1) is a new pVHL substrate identified in our screening (Figures 1B and 1C). SFMBT1 was identified as a transcriptional repressor component of the LSD1 demethylase complex that contains multiple MBT domains (Zhang et al., 2013a) and interacts with histone tails (Zhang et al., 2013a; Nady et al., 2012). However, SFMBT1 does not differentiate between unmodified and modified histone peptides (Zhang et al., 2013a). Therefore, there may be additional functions of SFMBT1 that remain uncharacterized. The role of SFMBT1 in cancer, especially in kidney cancer in its relation to *VHL*, has not been previously explored.

First, we examined SFMBT1 levels in pVHL null ccRCC cell lines (786-O, UMRC2, RCC4, and UMRC6), with or without pVHL restoration. In all the cell lines examined, pVHL restoration led to the downregulation of SFMBT1, phenocopying HIF2α regulation (Figure 1D). The regulation of SFMBT1 by pVHL may be independent of HIF signaling, because depletion of HIF1β or HIF2α by two independent CRISPR-Cas9 guide RNAs (sgRNAs) did not affect SFMBT1 protein levels in ccRCC cells (Figures S1A and S1B). It is also important to note that SFMBT2, a close family member of SFMBT1, was not regulated at the protein level by pVHL restoration in these cells (Figure S1C). We also depleted pVHL expression by using sgRNAs in the pVHL-expressing cell lines Caki-1 and HKC. Two independent sgRNAs against *VHL* led to SFMBT1 and HIF1α upregulation in these cells (Figure 1E). Canonical regulation of pVHL substrates is through hydroxylation, followed by recognition by the pVHL E3 ligase complex, resulting in ubiquitination and proteasomal degradation (Ivan et al., 2001; Jaakkola et al., 2001). To test whether the potential regulation of SFMBT1 by pVHL depends on its hydroxylation, we treated control and HA-pVHL expressing 786-O, UMRC2, RCC4, and UMRC6 cells with

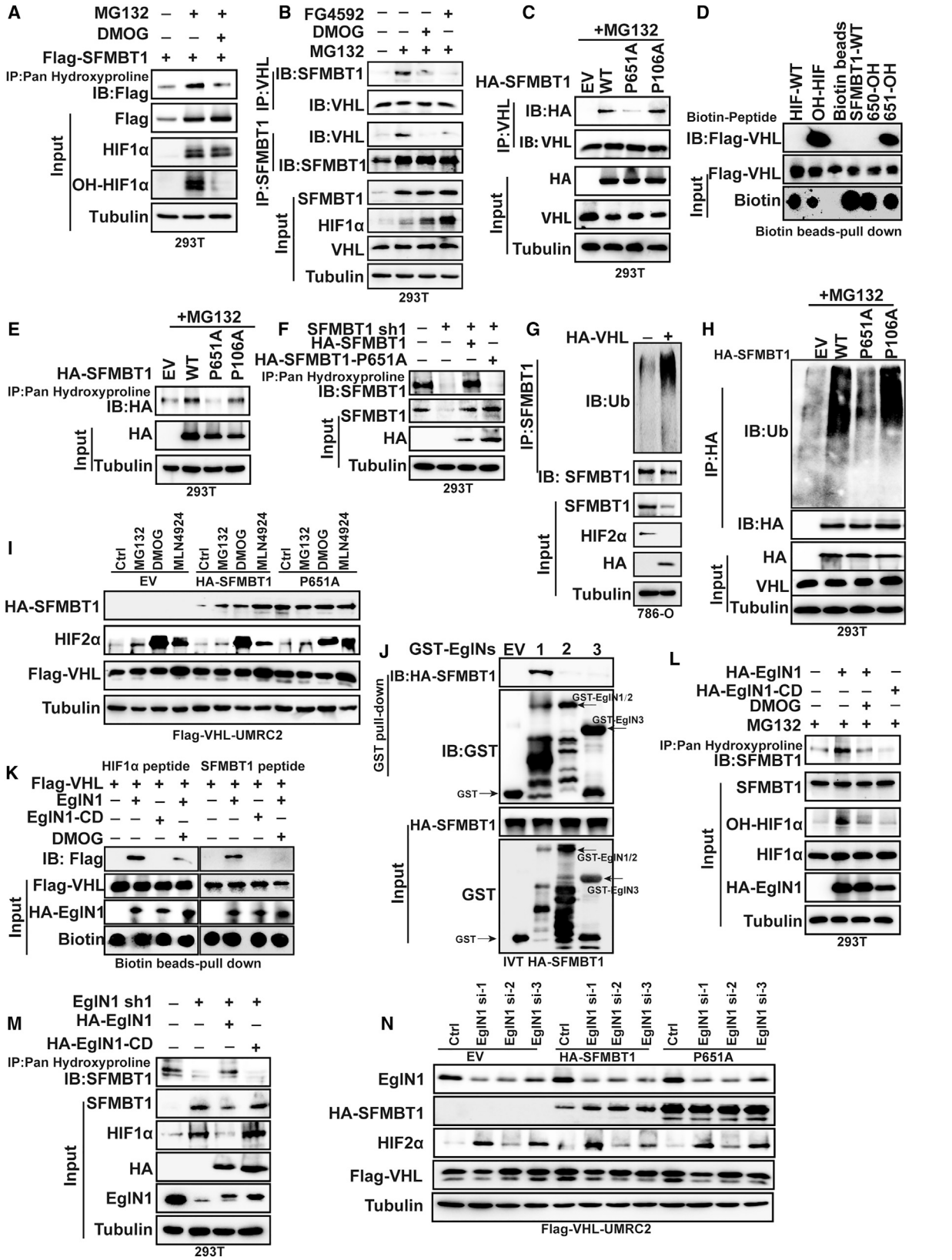

(legend on next page)

dimethyloxalylglycine (DMOG) or hypoxic conditions (1% O_2), both able to inhibit hydroxylation. Inhibition of hydroxylation induced SFMBT1 expression to a level comparable to that of cells lacking functional pVHL (Figure 1F). Similar results were observed for the canonical pVHL substrate HIF2α (Figure 1F), indicating that the negative regulation of SFMBT1 by pVHL is hydroxylation-dependent. In addition, treatment of HA-pVHL expressing cells with the proteasome inhibitor MG132 also led to SFMBT1 upregulation (Figure 1F), suggesting that SFMBT1 hydroxylation leads to pVHL-mediated proteasomal degradation. Strengthening the observation from pVHL null ccRCC cell lines that SFMBT1 regulation is dependent on hydroxylation and proteasomal degradation, treatment of pVHL-expressing renal cells (Caki-1, HKC, or 293T) with MG132, DMOG, or hypoxia also resulted in upregulation of SFMBT1 expression (Figure 1G).

Potential Prolyl Hydroxylation Regulates SFMBT1 Binding and Ubiquitination by pVHL

Our results suggest that SFMBT1 may undergo hydroxylation and regulation by pVHL, which is further strengthened by the ability of pan-hydroxyproline antibody to pull-down hydroxylated SFMBT1 in the presence of MG132, an effect abrogated by concurrent MG132 and DMOG treatment (Figure 2A). We further examined the binding between endogenous SFMBT1 and pVHL by reciprocal immunoprecipitations in the presence or absence of prolyl hydroxylase inhibitors FG4592 or DMOG; decreased binding between SFMBT1 and pVHL was observed when prolyl hydroxylation was inhibited (Figure 2B). We observed similar results in 786-O cells with pVHL restoration (Figure S2A). Moreover, GST-pVHL was able to pull down *in vitro* translated SFMBT1, indicating that pVHL binds SFMBT1 directly (Figure S2B). GST pull-down of endogenous SFMBT1 from 786-O cells further confirmed the binding between GST-pVHL and SFMBT1, which was diminished when cells were treated with either DMOG or FG4592 (Figure S2C). Next, we aimed to identify the potential SFMBT1 prolyl hydroxylation sites that mediate its binding and potential ubiquitination by pVHL. We overexpressed FLAG-tagged SFMBT1 in 293T cells, followed by treatment with either MG132 or MG132 together with DMOG and performed mass spectrometry (Figure S2D). Specifically, we were interested in those Proline sites displaying decreased hydroxylation levels upon DMOG treatment. To increase our confidence, we performed two independent experiments and sent these samples to two different mass spectrometry facilities for the identification of prolyl hydroxylation sites. From both sets of experiments, we identified only two common prolyl hydroxylation sites: Prolines 106 and 651 (Figures S2E-G). Next, we mutated SFMBT1 Prolines 106 and 651 to alanines (P106A and P651A). Whereas WT or P106A mutant SFMBT1 bound pVHL efficiently, P651A mutant binding to pVHL was impaired, suggesting that P651 is the major hydroxylation site recognized by pVHL (Figure 2C). Subsequently, we synthesized WT (SFMBT1-WT) or Proline 650/651 hydroxylated (P650-OH and P651-OH) SFMBT1 peptides and performed the binding assay with pVHL (Figure 2D). Only P651-OH peptide was able to bind with pVHL strongly, similar to hydroxylated HIF1α peptide (Figure 2D). We noticed that there was an adjacent Proline (P650) on SFMBT1 but synthesized P650-OH peptide failed to bind with pVHL (Figure 2D), suggesting that Proline 651 is the specific site undergoing hydroxylation leading to pVHL binding. Consistently, pan-hydroxylation IP of HA-tagged WT (WT), P106A, or P651A SFMBT1 followed by HA-SFMBT1 immunoblot showed that only P651A mutant abrogated the hydroxylation signal (Figure 2E). We also depleted endogenous SFMBT1 and restored with physiologically relevant levels of SFMBT1 WT or P651A SFMBT1 mutant followed by examination of SFMBT1 hydroxylation. Both SFMBT1 depletion and P651A mutation abrogated the hydroxylation signal (Figure 2F).

To examine whether pVHL regulates SFMBT1 via ubiquitination, we performed an *in vivo* ubiquitination assay in 293T cells transfected with HA-SFMBT1 in the presence or absence of exogenous FLAG-tagged pVHL. We observed a stronger HA-SFMBT1 ubiquitination with FLAG-pVHL expression, as well as decreased HA-SFMBT1 protein level (Figure S2H). We also confirmed this *in vivo* ubiquitination assay in pVHL-deficient 786-O renal cancer cells or isogenic cells reconstituted with HA-pVHL and observed an increase in endogenous SFMBT1 ubiquitination upon HA-pVHL expression (Figure 2G). To investigate whether P651 affects SFMBT1 ubiquitination by pVHL, we performed an *in vivo* ubiquitination assay in 293T cells.

Figure 2. SFMBT1 Stability Is Regulated by pVHL through EglN1 Hydroxylation

(A) Immunoprecipitaiton of cell lysates for the hydroxylated SFMBT1 from cells treated with MG132 or MG132 plus DMOG treatment.

(B) Immunoprecipitaiton and immunblots of cell lysates treated with indicated drugs overnight.

(C) Immunoprecipitaiton and immunblots of lysates from cells transfected with indicated plasmids followed by MG132 treatment.

(D) Binding between FLAG-pVHL and HIF1α or SFMBT1 peptides.

(E and F) Immunoprecipitaiton of lysates for the hydroxylated SFMBT1 in cells transfected (E) or transduced with plasmids or lentivirus indicated (F).

(G) Effect of HA-pVHL on ubiquitination of endogenous SFMBT1.

(H) Ubiquitination level of HA-SFMBT1 (WT), P651A, and P106A.

(I) Immunoblots for lysates of transduced HA-SFMBT1 and P651A in UMRC2 transduced with lentivirus expressing FLAG-pVHL (FLAG-VHL-UMRC2) followed by treatment with indicated drugs.

(J) GST-pull down assay between GST (EV) or GST-EglNs (EglN1, EglN2, and EglN3) and *in vitro* translated (IVT) HA-SFMBT1.

(K) Capture of biotinylated HIF1α (left panel) and SFMBT1 (right panel) peptides by FLAG-VHL after *in vitro* hydroxylation by IVT EglN1 (wide-type) or EglN1 catalytic dead variant (H314VD316/A314VA316, EglN1-CD). HIF1α peptide was used as positive control. Capture of peptides by FLAG-pVHL indicates hydroxylation of peptides by EglN1.

(L) Hydroxylation level of endogenous SFMBT1 in cells transfected with HA-EglN1 or EgLN1-CD, followed by MG132 or MG132 plus DMOG treatment.

(M) Immunoblots of immunoprecipitated samples to detect endogenous SFMBT1 hydroxylation in cells with EglN1 knockdown (sh1) as well as these cells restored with HA-EglN1 or catalytic dead mutant (HA-EglN1-CD).

(N) Immunoblots for lysates of transduced HA-SFMBT1 and P651A protein level in FLAG-VHL-UMRC2 cells transfected with control siRNA (Ctrl) or EglN1 siRNAs (si-1, si-2, and si-3).

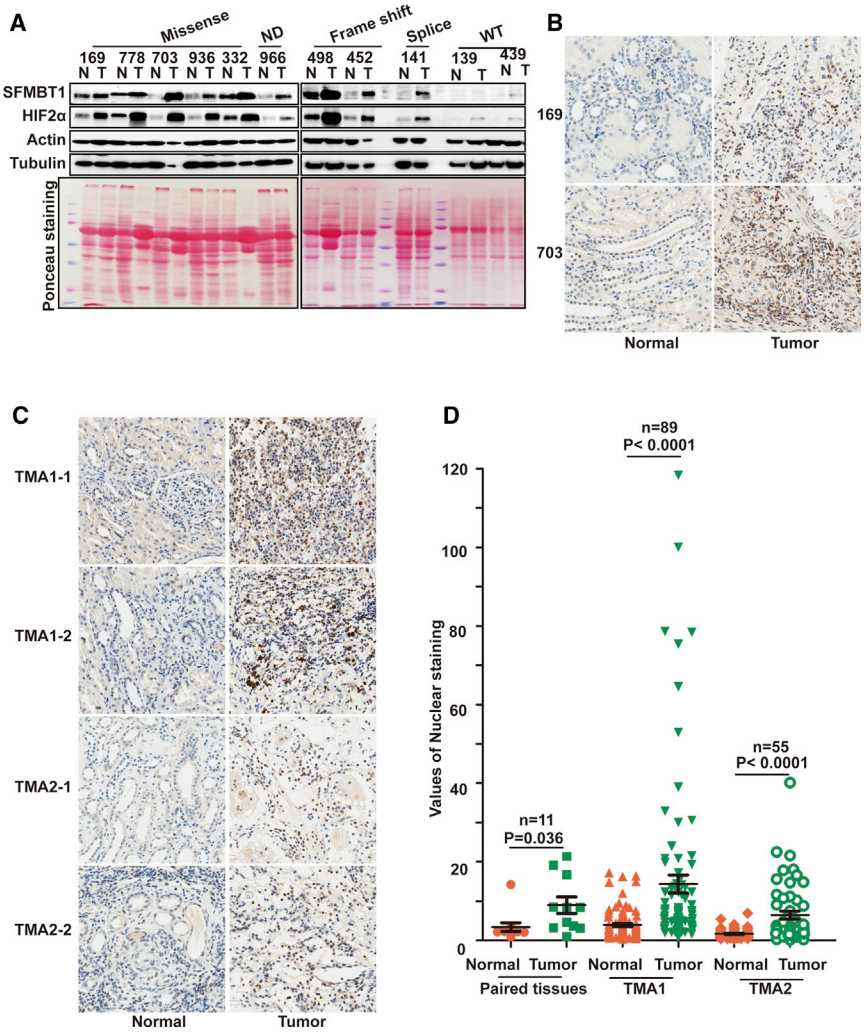

Figure 3. SFMBT1 Is Upregulated in ccRCC Patients

(A) Immunoblots for lysates from indicated ccRCC paired patient non-tumor (N) and tumor (T) tissues.

(B and C) Representative SFMBT1 immunohistochemical (IHC) staining for indicated ccRCC paired patient tissues (B) and tissue microarrays (TMA1 and TMA2) (C).

(D) Quantification of SFMBT1 nuclear staining for (B) and (C).

Consistent with western blot data showing SFMBT1 regulation by pVHL, pVHL promoted ubiquitination of WT or P106A, but not P651A SFMBT1 (Figure 2H). We also transduced FLAG-VHL UMRC2 cells with lentivirus expressing WT or P651A HA-SFMBT1, followed by treatment with MG132, MLN4924 (neddylation inhibitor that inhibits E3 ligase complex formation), or DMOG. WT HA-SFMBT1 was upregulated with these inhibitor treatments compared to control. Conversely, the P651A HA-SFMBT1 mutant was not affected by these inhibitors and was constantly upregulated compared to its WT counterpart (Figure 2I). Therefore, P651 is the primary site responsible for SFMBT1 hydroxylation and its regulation by the pVHL E3 ligase complex.

EglN1 Is the Primary Prolyl Hydroxylase that Regulates SFMBT1 Hydroxylation and Protein Stability in ccRCC

In order to test which prolyl hydroxylase family member may be responsible for SFMBT1 hydroxylation and regulation by pVHL, we first purified GST-EglN1, 2, and 3 recombinant protein followed by GST pull-down from 786-O cell lysates. By implementing an orthogonal strategy, we also performed GST pull-down of *in vitro* translated SFMBT1 from reticulocyte lysate. In both approaches, only GST-EglN1 could pull down SFMBT1 (Figures S2I and Figure 2J). Next, we performed an *in vitro* hydroxylation reaction with SFMBT1 unmodified peptide in the presence of *in vitro* translated EglN1 enzyme (Figure S2J). Only WT EglN1, but not its catalytic dead variant (EglN1-CD), promoted SFMBT1/HIF1α hydroxylation that was captured by pVHL (Figure 2K). EglN1-triggered hydroxylation of SFMBT1 or HIF1α was inhibited by co-incubation with DMOG (Figure 2K), further confirming that EglN1 promotes SFMBT1 hydroxylation followed by pVHL recognition. We also observed that WT EglN1, but not the EglN1-CD variant, promoted endogenous SFMBT1 hydroxylation that could be inhibited by DMOG treatment, as detected by immunoprecipitation with a pan-hydroxylation antibody (Figure 2L). We then depleted EglN1 and restored with physiologically relevant levels of EglN1 WT or catalytic dead (EglN1 CD) mutant and examined SFMBT1 hydroxylation. WT EglN1, but not the EglN1-CD variant, could promote SFMBT1 hydroxylation (Figure 2M). Consistently, EglN1 depletion by three different siRNAs led to increased exogenous WT SFMBT1 protein levels (Figure 2N). Mutation of the HA-SFMBT1 prolyl hydroxylation site P651A totally abrogated the regulation of HA-SFMBT1 by EglN1 depletion (Figure 2N). In addition, we also performed an *in vitro* hydroxylation assay with SFMBT1 peptide and EglN1 enzyme. Our results showed that the Km of SFMBT1 was 3.5 μM (Figures S2K and S2L). Together, our data suggest that EglN1 is the primary prolyl hydroxylase that hydroxylates SFMBT1 on Proline 651, which leads to pVHL binding and proteasomal degradation.

SFMBT1 Is Upregulated in ccRCC Patient Tumors

Next, to examine the physiological relevance of SFMBT1 in ccRCC, where most of patients carry *VHL* loss-of-function mutations, we analyzed 11 pairs of tumor and normal tissues from ccRCC patients. Most tumors carrying splice variant, missense, or frameshift mutations displayed consistent upregulation of SFMBT1 compared to paired normal tissues, which correlated

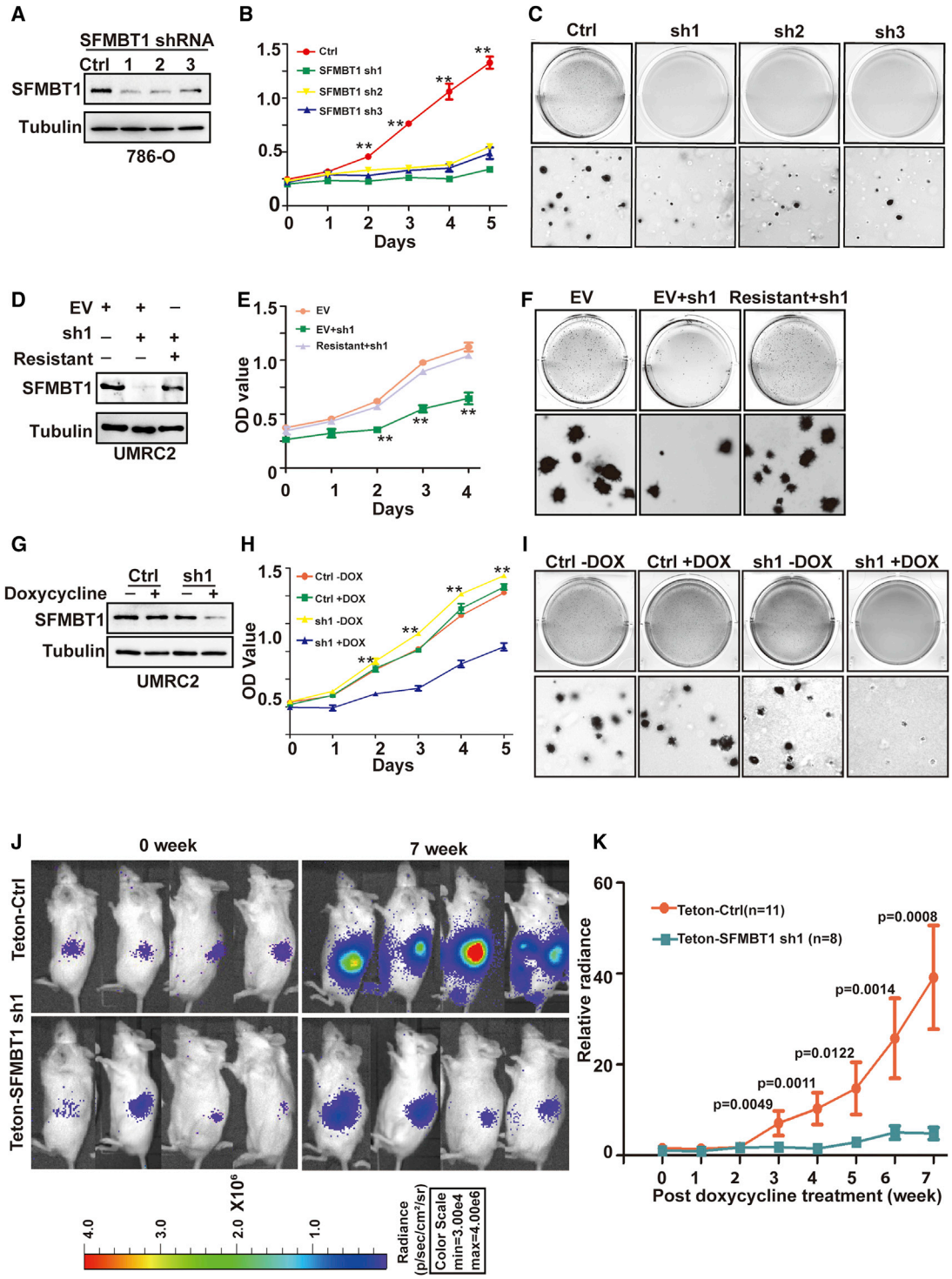

Figure 4. SFMBT1 Regulates ccRCC Cell Proliferation, Anchorage-Independent Growth, and Tumorigenesis

(A–C) Immunoblots for lysates (A), cell proliferation assays (B) and representative anchorage-independent growth assays (C) in cells transduced with lentivirus expressing either control shRNA (Ctrl) or SFMBT1 shRNAs (sh1, sh2 and sh3). * Ctrl versus SFMBT1 sh1/2/3; **p < 0.01.

(D–F) Immunoblots for lysates (D), cell proliferation assays (E), and representative anchorage-independent growth assays (F) in cells transduced with lentivirus expressing either control shRNA (Ctrl) or SFMBT1 sh1, followed by infection with lentivirus encoding empty vector (EV) or HA-SFMBT1 sh1-resistant (resistant). * EV+sh1 versus EV/Resistant+sh1; **p < 0.01; ***p < 0.001.

(legend continued on next page)

well with HIF2α levels in these patients (Figure 3A). Conversely, ccRCC tumors with wild-type *VHL* did not display distinctive upregulation of SFMBT1 or HIF2α (Figure 3A). We next examined SFMBT1 mRNA in the 11 pairs of normal and tumor tissues. Among them, 8 showed comparable mRNA levels between normal and tumors, one pair showed decreased SFMBT1 mRNA in the tumor, and the other 2 pairs displayed increased SFMBT1 mRNA in tumors (Figure S3A). Therefore, VHL-loss-induced SFMBT1 protein upregulation is likely due to protein stabilization. We next performed immunohistochemical (IHC) staining for these tumors and found that SFMBT1 expression was increased in the nuclei of tumors with *VHL* loss-of-function mutations compared to their respective adjacent normal tissues (Figure 3B). We also examined SFMBT1 protein levels in tumors from a previously generated ccRCC mouse model with pVHL loss (Bailey et al., 2017); SFMBT1 was upregulated in multiple ccRCC tumors compared to normal kidney tissues (Figure S3B), suggesting the importance of SFMBT1 in human and mouse ccRCC pathogenesis. To corroborate our IHC staining results for SFMBT1 in ccRCC patient tumors, we also stained two sets of ccRCC tissue microarrays (TMAs) for SFMBT1. Consistent with our previous IHC staining in individual ccRCC tumors, SFMBT1 showed higher nuclear intensity in tumors compared to normal controls in both TMA sets, as reflected by representative IHC staining images as well as quantitative analyses (Figures 3C and 3D).

SFMBT1 Controls ccRCC Cell Proliferation, Anchorage-Independent Growth, and Tumorigenesis

SFMBT1 was initially described as a transcriptional repressor (Wu et al., 2007). However, the mechanisms underlying this function, as well as the potential implication of SFMBT1 in cancer, remain largely unexplored. Given the important role of pVHL in ccRCC and the identification of SFMBT1 as a target for pVHL, we aimed to uncover the function of SFMBT1 in ccRCC. To this end, SFMBT1 expression in pVHL null 786-O renal cancer cells was depleted using three different validated hairpins (1, 2, and 3) in a PLKO-based lentiviral vector. SFMBT1 depletion significantly decreased cell proliferation (Figures 4A and 4B) and 3D soft-agar growth (Figures 4C and S4A). We also observed a similar cell proliferation and 3D soft agar growth defect upon SFMBT1 depletion in another ccRCC cell line, UMRC2 (Figures S4B–S4E). To further confirm that this phenotype was due to the on-target effects of SFMBT1 hairpins, we depleted SFMBT1 expression and then co-transfected UMRC2 cells with an shRNA-resistant SFMBT1 expression plasmid (Figure 4D). Whereas the SFMBT1 shRNA decreased cell proliferation and colony formation, shRNA-resistant SFMBT1 overexpression efficiently rescued the phenotype (Figures 4E and 4F; Figure S4F), suggesting that these phenotypes were due to on-target consequences of SFMBT1 depletion.

To examine whether SFMBT1 was important for ccRCC tumor growth, we constructed 786-O cells expressing an inducible SFMBT1 shRNA, which efficiently depleted SFMBT1 levels upon doxycycline addition in ccRCC cell lines (Figure 4G). SFMBT1 depletion also showed decreased cell proliferation and soft-agar growth upon doxycycline addition in UMRC2 cells (Figures 4H and 4I; Figure S4G) and 786-O cells (Figures S4H–S4K). Next, either control or SFMBT1 shRNA (sh1) cells were orthotopically injected into the renal capsules of NOD scid gamma (NSG) mice. Upon confirmation of tumor growth *in vivo* by consecutive weekly bioluminescence imaging, we administered doxycycline to induce SFMBT1 hairpin expression and monitored live tumor growth. Whereas cells expressing control hairpins grew readily during the seven weeks after the addition of doxycycline, SFMBT1 hairpin-expressing cells failed to proliferate *in vivo* (Figures 4J and 4K). Taken together, our results suggest that SFMBT1 is important for ccRCC both *in vitro* and *in vivo*.

SFMBT1 Activates Gene Expression in ccRCC

To investigate how SFMBT1 affects ccRCC tumorigenesis, we performed chromatin immunoprecipitation followed by high-throughput sequencing (ChIP-seq) to assess the genomic localization of SFMBT1 in ccRCC. 3073 binding sites were found, of which 91% overlapped with H3K27ac, 85% with H3K4me3, and only 12% with H3K4me1 (Figure S5A), suggesting that SFMBT1 binds preferentially to active gene promoters (Shlyueva et al., 2014). In addition, there was limited overlap between SFMBT1 and either HIF2α or HIF1β binding sites, indicating that SFMBT1 regulates distinctive downstream events from HIF2α or HIF1β (Figures 5A and S5A). To identify the genes that SFMBT1 may preferentially activate, we performed RNA-seq with two independent SFMBT1 siRNAs and focused on SFMBT1 positively regulated genes. We compared these genes to those activated by HIF2α, as reported in a previous study (Yao et al., 2017). There was very little overlap between SFMBT1 and HIF2α activated genes (Figure S5B), further suggesting that SFMBT1 promotes ccRCC tumorigenesis through HIF2α-independent signaling. It is important to note that these HIF2α activated genes may be an underrepresentation that could result from incomplete depletion of HIF2α by siRNA. However, an analysis of enriched transcription factor motifs within SFMBT1 binding sites did not reveal a HIF motif, and instead showed enrichment for RBPJ1, MYC, and AP-1, among others (Figure S5C).

Next, to identify the critical SFMBT1 target genes involved in ccRCC tumorigenesis, we applied the following stringent criteria for genes: (1) displayed positive regulation by SFMBT1 (downregulated by both SFMBT1 siRNAs) and exhibited SFMBT1 binding in the promoter (±5 kb from transcription start site), resulting

(G–I) Immunoblots for lysates (G), cell proliferation assays (H), and representative anchorage-independent growth assays (I) in UMRC2 luciferase stable cells tranduced with lentivirus expressing either Teton control shRNA (Ctrl) or Teton-SFMBT1 shRNA1 (sh1), and treated with or without doxycycline as indicated. * sh1+dox versus sh1-dox/Ctrl-dox/Ctrl+dox; **$p < 0.01$.

(J and K) Representative bioluminescence imaging of before (0 week) and 7 weeks post-doxycycline treatment (J) and quantification of post-doxycycline treatment bioluminescence imaging (K) from 786-O luciferase stable cells transduced with lentivirus expressing either Teton control (Teton-Ctrl) or Teton-SFMBT1 sh1 that were injected orthotopically into the renal sub-capsule of NOD SCID gamma (NSG) mice.

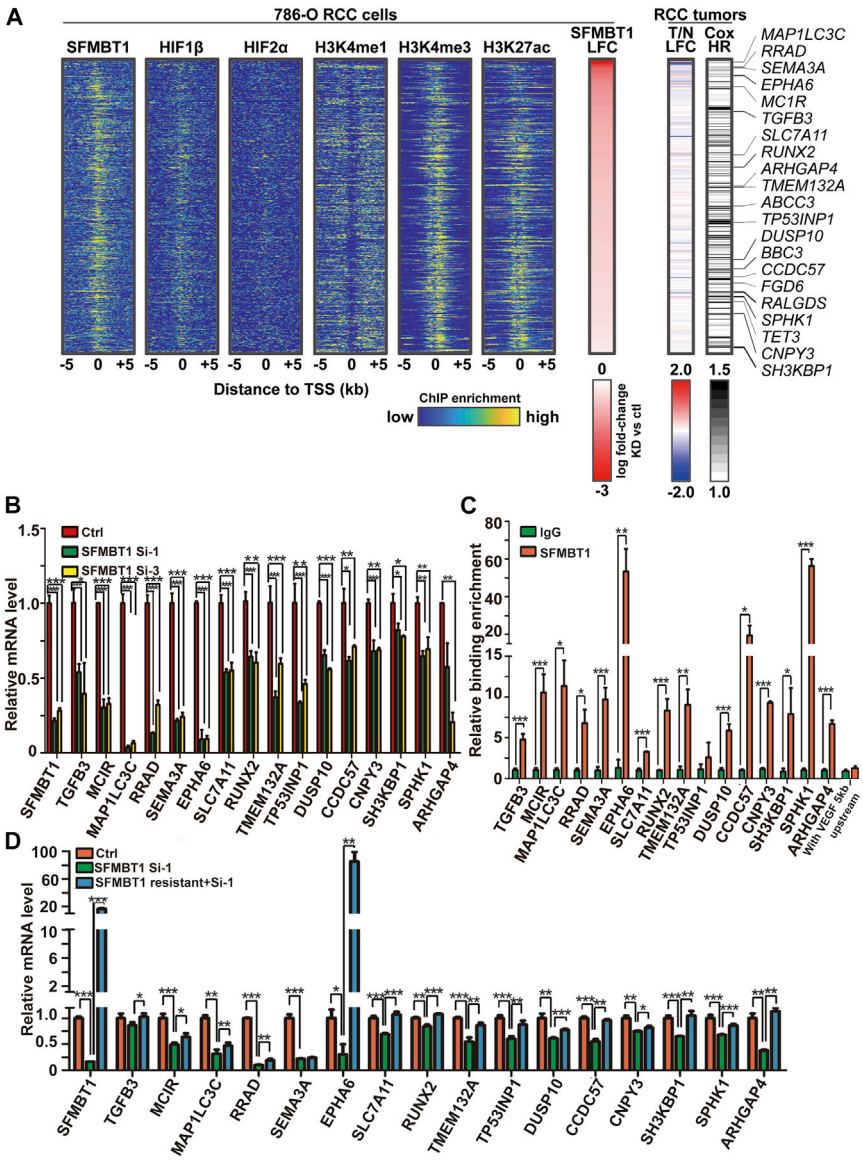

Figure 5. Identification of Critical SFMBT1 Direct Target Genes in ccRCC

(A) Integrated analyses of ChIP-seqs, including SFMBT1, HIF1β, HIF2a, H3K4me1, H3K4me3, and H3K27ac, signals expressed as relative to input control when available. Log2 fold change (LFC) for SFMBT1 RNA-seq with two different siRNAs; Log2 fold change for kidney clear cell carcinoma (KIRC) tumor (T) versus normal (N) in TCGA database as well as patient prognosis (Cox HR value). Critical target genes were marked on the right.

(B) qRT-PCR quantification of SFMBT1 target genes from 786-O cells transfected with SFMBT1 control siRNA (Ctrl) or siRNAs (si-1 and si-3)

(C) ChIP-qPCR validation of binding for SFMBT1 at 16 target gene promoters compared to IgG control. VEGF 5kb upstream promoter sequence as a negative locus control for SFMBT1.

(D) qRT-PCR quantification of SFMBT1 target genes from 786-O cells transduced with lentivirus expressing either control or SFMBT1 si1-resistant (SFMBT1 resistant) HA-SFMBT1, followed by transfection with control siRNA (Ctrl) or SFMBT1 siRNA1 (si-1).

For all the panels, *p < 0.05; **p < 0.01; ***p < 0.001.

in 516 genes (Figure S5D); (2) contained H3K4me3 and H3K27ac ChIP-seq in the promoter (±5 kb from transcription start site) (Figure 5A); (3) showed elevated expression in ccRCC patient tumors compared to normal in TCGA Kidney Clear Cell Carcinoma (KIRC) dataset (Cancer Genome Atlas Research Network, 2013) (Figure 5A); and (4) their high expression predicted worse prognosis in ccRCC patients (Figure 5A). By combining all these parameters, we narrowed down the direct SFMBT1 target gene list to 20 genes (Figures 5A and S5E). Among them, 16 genes displayed reliable gene expression as well as regulation by SFMBT1 (Figure 5B). Next, we further confirmed SFMBT1 binding on these target gene promoters by ChIP-qPCR (Figure 5C). In addition, we performed RT-PCR to examine the potential rescue of gene expression by siRNA resistant SFMBT1 cDNA clones. In nearly all target genes (15 out of 16), expression was completely/partially rescued by the introduction of siRNA-resistant SFMBT1 (Figure 5D), further strengthening our hypothesis that these are direct SFMBT1 target genes contributing to ccRCC pathogenesis.

SPHK1 Is the Critical SFMBT1 Target Gene that Contributes to ccRCC Tumorigenesis

We examined the ChIP-seq signals of SFMBT1, HIF2α, HIF1β, H3K4me1, H3K4me3, and H3K27Ac for each of these 16 genes (Figure S5F) and observed particularly robust binding by SFMBT1 to sphingosine kinase 1 (*SPHK1*), which coincided with strong H3K4me3 and H3K27ac enrichment, but not HIF2α or HIF1β (Figures 6A and 5A; Figure S5F). Our ChIP-qPCR further confirmed the strong enrichment of SFMBT1 on the *SPHK1* gene promoter (Figure 5C).

SPHK1 is a kinase that catalyzes the phosphorylation of sphingosine to form sphigosine-1-phosphate (S1P). By analyzing TCGA data, we found that *SPHK1* expression was higher in tumors compared to normal tissues, and its high expression predicted worse prognosis in ccRCC (Figures S6A and S6B). Consistent with this finding, we also found that higher stage (III and IV) tumors expressed higher levels of *SPHK1* mRNA compared to lower stage (I and II) tumors and to normal tissue (Figure S6C). Therefore, we decided to focus our efforts on characterizing the role of SPHK1 in SFMBT1 signaling in ccRCC. SFMBT1, but not HIF2α or HIF1β, occupies the proximal promoter region of *SPHK1* (Figure 6A). Consistent with the reduction in SFMBT1 following pVHL restoration in pVHL null ccRCC cell lines (Figure 1D), SPHK1 protein levels were also reduced when pVHL was restored (Figure S6D).

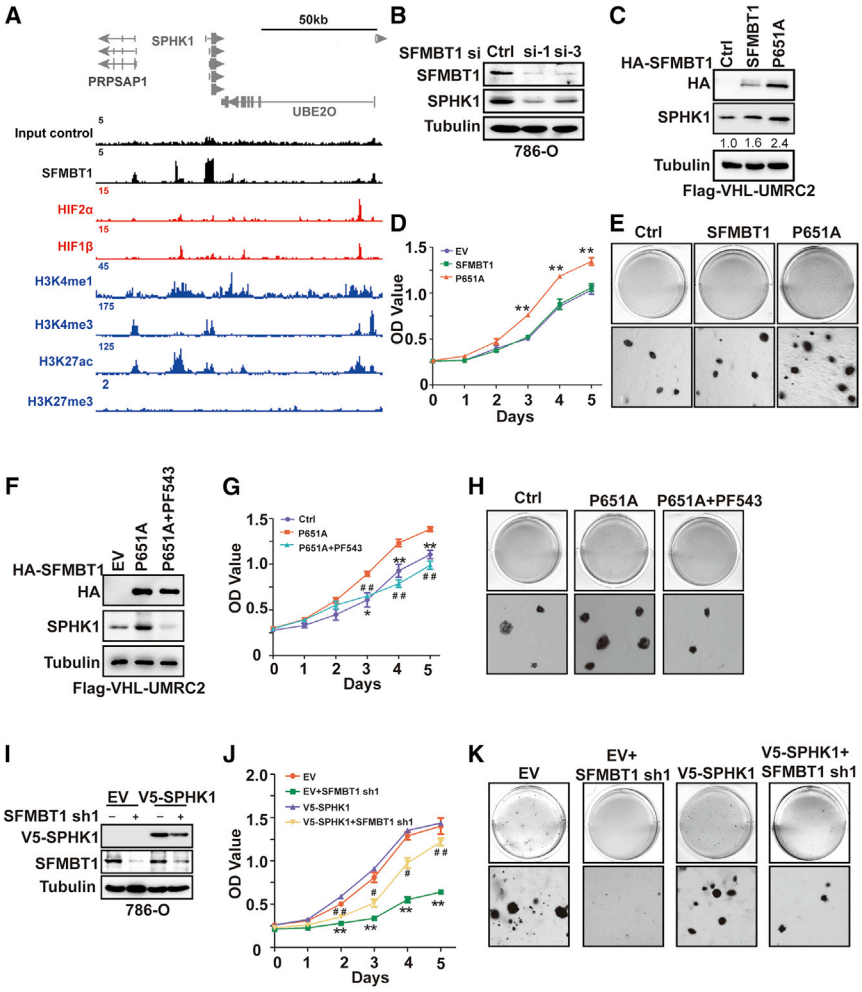

Figure 6. SPHK1 Is an SFMBT1 Direct Target Gene in ccRCC

(A) ChIP-seq binding peaks on SPHK1 for SFMBT1, HIF2α, HIF1β, H3K4me1, H3K4me3, H3K27ac, and H3K27me3.

(B) SPHK1 protein level in cells transfected with control siRNA (Ctrl) or SFMBT1 si-1 and si-3.

(C–E) Immunoblots for lysates (C), cell proliferation assays (D) and representative anchorage-independent growth assays (E) in cells infected with lentivirus encoding either empty vector (EV), HA-SFMBT1, or P651A. * EV/SFMBT1 versus P651A; **p < 0.01. The values listed below the blots (C) indicate the relative SPHK1 protein levels with tubulin normalization.

(F–H) Immunoblots for lysates (F), cell proliferation assays (G) and representative anchorage-independent growth assays (H) in cells infected with lentivirus encoding either empty vector (EV), P651A with or without PF543 treatment. * P651A versus Ctrl; # P651A+PF543 versus Ctrl. */#, p < 0.05; **/# #, p < 0.01.

(I–K) Immunoblots for lysates (I), cell proliferation assays (J) and representative anchorage-independent growth assays (K) in cells transduced with lentivirus expressing either SFMBT1 shRNA control (Ctrl) or SFMBT1 sh1, followed by infection with lentivirus encoding either empty vector (EV) or v5-SPHK1. * EV+shSFMBT1 sh1 versus EV; # v5-SPHK1+SFMBT1 sh1 versus EV. */#, p < 0.05; **/# #, p < 0.01.

SFMBT1 depletion by two independent siRNAs in pVHL null ccRCC cells led to decreased SPHK1; this effect was rescued by the expression of the siRNA-resistant version of SFMBT1 (Figures 6B and S6E), but was unaffected by HIF2α or HIF1β depletion (Figures S6F and S6G) in 786-O cells. In addition to SFMBT1 knockdown experiments, we also overexpressed control, WT, or P651A mutant HA-SFMBT1 in UMRC2 cells with FLAG-pVHL restored. As expected, P651A HA-SFMBT1 protein level was higher than that of its wild-type counterpart (Figure 6C), most likely due to the inability of P651A HA-SFMBT1 to be marked for degradation by pVHL. Consistently, ccRCC cells expressing P651A HA-SFMBT1 displayed higher SPHK1 protein levels, which corresponded to increased cell proliferation and soft-agar growth compared to either control vector or WT SFMBT1-infected cells (Figures 6C–6E; Figure S6H). Next, we overexpressed control, WT, or P651A mutant HA-SFMBT1 in the VHL WT cell line HKC, and saw similar effects here (Figure S6I–S6L) to that of FLAG-pVHL restored UMRC2 cells (Figure 6C). We also cultured these cells under hypoxia; hypoxia led to an increase in protein levels of endogenous SFMBT1 and exogenous WT SFMBT1, but not the P651A SFMBT1 mutant, suggesting that Proline 651 is the major hydroxylation site important for its protein level regulation (Figure S6M). Additionally, we found that EV and WT SFMBT1 expressing HKC cells grew faster under hypoxia compared to normoxia. However, the cell proliferation rate for P651A expressing HKC cells was not affected by hypoxia compared to normoxia (Figure S6N).

Next, we aimed to determine whether SPHK1 mediated the effect of SFMBT1 on ccRCC cell proliferation. For this purpose, we utilized the specific SPHK1 inhibitor PF543 in ccRCC cells (Schnute et al., 2012), which was shown to induce SPHK1 proteasomal degradation (Byun et al., 2013; Baek et al., 2013). PF543 treatment resulted in decreased cell proliferation and 3D soft-agar growth in 786-O and UMRC2 cells in a dose-dependent manner (Figure S6O–S6V). Whereas P651A SFMBT1 expression upregulated SPHK1 protein level, this effect was abrogated by PF543 (Figure 6F). ccRCC cells expressing P651A HA-SFMBT1 displayed increased cell proliferation and 3D soft-agar growth (Figures 6G and 6H; Figure S6W); this effect was also disrupted by the co-treatment with PF543. We also depleted SFMBT1 by shRNAs followed by either control or V5-SPHK1 overexpression; V5-SPHK1 overexpression could rescue the effect of SFMBT1 depletion on cell proliferation and soft-agar growth (Figures 6I–6K; Figure S6X). More importantly, PF543 did not grossly affect cell proliferation in HKC cells as measured by either a 2-D MTS assay or 3D soft agar assay (Figures S7A–S7D). We also found that depleting SPHK1 by two

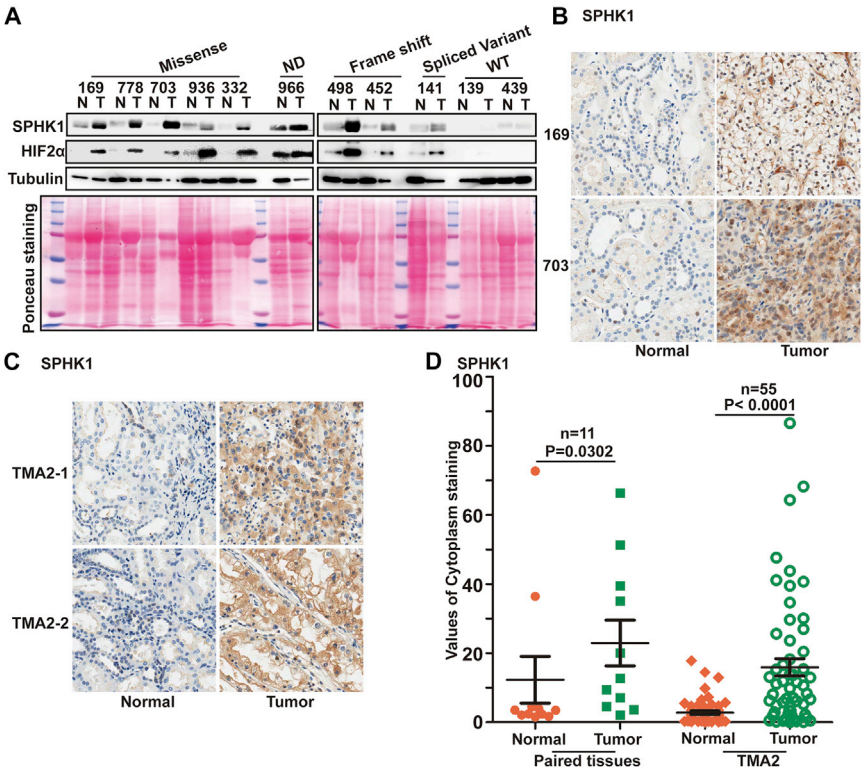

Figure 7. SPHK1 Is Upregulated in ccRCC Patients

(A) Immunoblots for lysates in indicated ccRCC paired patient non-tumor (N) and tumor (T) tissues.

(B and C) Representative SPHK1 immunohistochemical (IHC) staining for indicated ccRCC paired patient tissues (B) and tissue microarrays (TMA2) (C).

(D) Quantification of SPHK1 cytoplasm staining for (B) and (C).

(E and F) Schematic diagram of relationship of pVHL, SFMBT1, and SPHK1.

different shRNAs inhibited 786-O and UMRC2 cell proliferation and soft-agar growth (Figures S7E–S7L). In summary, SPHK1 is a major mediator for the oncogenic phenotype of SFMBT1 on ccRCC cell proliferation.

SPHK1 Is Upregulated in ccRCC Patient Tumors and Controls Tumorigenesis

Next, to examine the physiological relevance of SPHK1 in ccRCC, we assessed SPHK1 and HIF2α protein levels in the 11 pairs of normal and tumor tissues from ccRCC patients (same as in Figure 4A). Most tumors displayed consistent upregulation of SPHK1 compared to paired normal tissues, which correlated well with HIF2α levels in these patients (Figure 7A). We next performed immunohistochemical (IHC) staining for these tumors and found that SPHK1 expression was increased in the cytoplasm of tumors with *VHL* loss-of-function mutations compared to their respective adjacent normal tissues (Figure 7B). To corroborate our IHC staining results for SPHK1 in ccRCC patient tumors, we also stained one set of ccRCC tissue microarrays (TMA2) for SPHK1 (same as in Figures 4C and 4D). Consistent with our previous IHC staining in individual ccRCC tumors, SPHK1 showed higher cytoplasmic staining intensity in tumors compared to normal controls, as reflected by representative IHC staining images as well as quantitative analyses (Figures 7C and 7D).

We analyzed the correlation of SPHK1 and SFMBT1 staining intensity in the combined dataset of our 11 paired tissues and TMA2. As shown, in normal samples, SPHK1 and SFMBT1 staining showed a significant correlation (Spearman correlation = 0.33, p = 0.007358) (Figure S7M). In tumor samples, there was a trend that SPHK1 and SFMBT1 correlated but it did not reach statistical significance (Spearman correlation = 0.226, p = 0.06994) (Figure S7N). Next, we examined whether SPHK1 was important for ccRCC tumor growth by orthotopically injecting 786-O cells into the renal capsules of NSG mice. Upon confirmation of tumor growth *in vivo*, we treated mice with PF543 to inhibit SPHK1. PF543 did inhibit SPHK1 but not SPHK2 expression level (Figure S7O) *in vivo*. PF543 also inhibited ccRCC tumor growth *in vivo* (Figures S7P and S7Q). Taken together, our results suggest that SPHK1 is important for ccRCC tumor growth *in vivo*.

DISCUSSION

SFMBT1 is regulated by pVHL through a prolyl hydroxylation- and proteasomal degradation-dependent mechanism (Figure 7E). Loss of pVHL leads to increased SFMBT1 level, which promotes cell proliferation and xenograft tumor growth in ccRCC cells (Figure 7F). Our results provide some new evidence that targeting the SFMBT1-SPHK1 axis decreases kidney cancer fitness in HIF2α-inhibitor-resistant cancer cell lines (such as UMRC2).

VHL is the predominant tumor suppressor gene in renal cancer. The canonical pathway for pVHL E3 ubiquitin ligase complex activity is that *VHL* loss leads to HIF2α accumulation, which promotes renal cell malignant transformation (Kondo et al., 2003;

Kondo et al., 2002). However, recent developments have helped understand the function of pVHL from several different perspectives. Emerging literature suggests the existence of additional pVHL substrates beside HIFs (Li and Kim, 2011), such as NDRG3 (Lee et al., 2015) and ZHX2 (Zhang et al., 2018). Therefore, the function of pVHL appears to be multi-faceted, including both E3 ligase-dependent and -independent functions that reach beyond canonical HIF signaling (Zhang and Zhang, 2018). However, the identification of novel and relevant pVHL E3 ligase complex substrates remains a challenge. One reason is that a unique modification of pVHL substrates (such as prolyl hydroxylation) may be required for pVHL recognition. Therefore, such proteins may not be easily identified by traditional pull-down approaches in the case of low hydroxylated protein levels. Another reason could be the low abundance of these substrates in cell lysates, similar to the case of very low basal levels of HIFα factors. By using an *in vitro* expression strategy with approximately 17,000 genes divided into 700 pools (24 genes/pool), coupled with a GST-pVHL binding screen, we identified novel pVHL binding partners, as well as potential pVHL substrates. More importantly, our strategy can be broadly applied to search for other E3 ligase substrates.

We have accumulated a substantial amount of evidence showing that SFMBT1 is a potent oncogene and transcriptional regulator in kidney cancer in an HIF-independent manner. However, some questions remain to be answered. SFMBT1 Proline 651, the major hydroxylation site that contributes to the protein stability regulated by pVHL, is located outside of its MBT domains. It remains unclear whether the oncogenic phenotype of SFMBT1 is dependent on its MBT domains. SFMBT1 is considered to be a component of polycomb-repressive complex and is largely considered to be a transcription repressor (Sauvageau and Sauvageau, 2010). Specifically, SFMBT1 was shown to form a complex with LSD1 and CoREST in cells (Zhang et al., 2013a; Tang et al., 2013), though our data show that SFMBT1 both activated and repressed gene expression. We have not examined SFMBT1 in other cancer types since VHL loss is primarily restricted to kidney cancer; however, this will be explored further in future studies. It is also intriguing that SFMBT1 binding sites were enriched for motifs corresponding to transcription factors RBPJ1, MYC, and AP-1. RBPJ1 was reported to be a transcriptional activator for Notch signaling (Nam et al., 2006; Tani et al., 2001). pVHL loss was shown to activate Notch signaling in renal cancer (Sjölund et al., 2008). It is possible that the pVHL-SFMBT1-RBPJ1 axis may be able to modulate Notch activity in renal cancer, though this remains to be determined.

S1P signaling, acting downstream of SPHK1, plays an important role in diseases such as cancer and inflammatory diseases (Kunkel et al., 2013). The anti-S1P antibody was previously identified to be a novel therapeutic option for VEGFR tyrosine kinase inhibitor (TKI)-resistant renal cancer (Zhang et al., 2015). VEGF/VEGFR signaling acts downstream of HIF2α. One of the potential reasons for the VEGFR TKI resistance in renal cancer could be SPHK1 regulation by pVHL loss in an SFMBT1-dependent, but HIF2α-independent manner. It is important to point out that there may be other downstream targets of SFMBT1 that may be functionally important in kidney cancer, which remains to be determined.

During the preparation of our manuscript, a new study suggested a lack of evidence for the hydroxylation of non-HIF prolyl hydroxylase substrates by prolyl hydroxylases *in vitro* (Cockman et al., 2019). Our current study did perform EglN1-mediated hydroxylation with SFMBT1 peptide *in vitro*, and we found that there was increased hydroxylation signal with various concentrations of SFMBT1 peptides, albeit to much weaker extent compared to HIFα peptide. We also performed various experiments *in vivo* under physiologically relevant conditions to corroborate our *in vitro* data supporting the potential for SFMBT1 hydroxylation. However, we acknowledge that our assay did not measure the percentage of SFMBT1 hydroxylation *in vitro* or *in vivo*, which remains to be determined in future studies. However, this recently published study suggests that we will need a more rigorous approach to establish that SFMBT1 is indeed a bona fide EglN1 substrate, which we recognize as a limitation of our current study.

In summary, the most important tumor suppressor in kidney cancer, pVHL, appears to regulate multiple oncogenic signaling pathways in parallel. Whereas HIF2α is a well-established contributor to kidney cancer, SFMBT1 may represent another important oncogenic signaling pathway that could be responsible for a significant portion of renal tumors that do not respond to HIF2α inhibitor or multi-tyrosine kinase inhibitors (including Sorafenib and Axitinib). Since currently no potent SFMBT1 inhibitor is available, targeting its downstream target gene *SPHK1* with SPHK1 inhibitors, either alone or in combination with HIF2α pathway inhibitors, may represent a new therapeutic avenue for kidney cancer treatment.

STAR★METHODS

Detailed methods are provided in the online version of this paper and include the following:

- KEY RESOURCES TABLE
- LEAD CONTACT AND AVAILABILITY
- EXPERIMENTAL MODEL AND SUBJECT DETAILS
  - Orthotopic Tumor Growth
- METHOD DETAILS
  - Genome-Wide Screening
  - *In vitro* decarboxylation assay
  - Human ccRCC paired tissues
  - IHC and TMA
  - LC-MS/MS analysis
  - Transfection, Virus Production and Infection
  - Cell Proliferation Assays and Anchorage-Independent Growth assay
  - Immunoprecipitation and GST pull-down assay
  - Ubiquitination assay
  - *In vitro* hydroxylation followed by VHL binding assay
- QUANTIFICATION AND STATISTICAL ANALYSIS
  - RNA-Seq analysis
  - TCGA data
  - Chromatin immunoprecipitation and Integrated analysis
  - Statistical analysis
- DATA AND CODE AVAILABILITY

SUPPLEMENTAL INFORMATION

Supplemental Information can be found online at https://doi.org/10.1016/j.molcel.2020.01.009.

ACKNOWLEDGMENTS

We thank Dr. William G. Kaelin, Jr., for his support as the initial screening was performed by Q.Z. in Dr. Kaelin's lab in collaboration with Dr. Kirschner's lab with support from NCI R01 CA068490. We thank UNC LCCC Tissue Procurement Facility, UNC Animal Studies Core, and UNC Translational Pathology Laboratory for excellent help. This work was supported in part by the National Cancer Institute (Q.Z., R01CA211732 and R21CA223675) and Cancer Prevention and Research Institute of Texas (CPRIT, RP190058 to Q.Z.). J.M.S. and T.S.P. were supported by The Eunice Kennedy Shriver National Institute of Child Health and Human Development (U54HD079124) and NINDS (P30NS045892). Q.Z. is an American Cancer Society Research Scholar, CPRIT Scholar in Cancer Research, V Scholar, Kimmel Scholar, Susan G. Komen Career Catalyst awardee, and Mary Kay Foundation awardee. Q.Z. is also supported by Kidney Cancer Research Alliance (KCCure). This research is based in part upon work conducted using the UNC Proteomics Core Facility, which is supported in part by P30 CA016086 Cancer Center Core Support Grant to the UNC Lineberger Comprehensive Cancer Center.

AUTHOR CONTRIBUTIONS

Q.Z., T.W., and M.W.K. conceived the project. X.L. and Q.Z. designed, performed and interpreted experiments, and co-wrote the paper. J.M.S. and T.S.P. contributed to RNA, ChIP-seq bioinformatics analyses. J.M.S. also helped with the paper editing. H.X., M.L., and K.G. provided critical guidance and helps on IHC and TMA. L.H. contributed to *in vitro* decarboxylation assay. J.W. performed some cell proliferation and anchorage-independent growth assay. G.Z. provided purified proteins. F.C. contributed to patient prognosis data analysis. X.T. contributed to statistical analysis. L.H. helped with LC-MS/MS analysis. T.W. and M.W.K. contributed to genome-wide screening. W.Y.K. provided ccRCC mouse model. A.S.B. helped with guidance for critical experiments and paper writing.

DECLARATION OF INTERESTS

The authors declare no competing interests.

Received: June 11, 2019
Revised: November 9, 2019
Accepted: January 1, 2020
Published: February 4, 2020

REFERENCES

Ayad, N.G., Rankin, S., Ooi, D., Rape, M., and Kirschner, M.W. (2005). Identification of ubiquitin ligase substrates by in vitro expression cloning. Methods Enzymol. *399*, 404–414.

Baek, D.J., MacRitchie, N., Pyne, N.J., Pyne, S., and Bittman, R. (2013). Synthesis of selective inhibitors of sphingosine kinase 1. Chem. Commun. (Camb.) *49*, 2136–2138.

Bailey, S.T., Smith, A.M., Kardos, J., Wobker, S.E., Wilson, H.L., Krishnan, B., Saito, R., Lee, H.J., Zhang, J., Eaton, S.C., et al. (2017). MYC activation cooperates with Vhl and Ink4a/Arf loss to induce clear cell renal cell carcinoma. Nat. Commun. *8*, 15770.

Bullard, J.H., Purdom, E., Hansen, K.D., and Dudoit, S. (2010). Evaluation of statistical methods for normalization and differential expression in mRNA-Seq experiments. BMC Bioinformatics *11*, 94.

Byun, H.S., Pyne, S., Macritchie, N., Pyne, N.J., and Bittman, R. (2013). Novel sphingosine-containing analogues selectively inhibit sphingosine kinase (SK) isozymes, induce SK1 proteasomal degradation and reduce DNA synthesis in human pulmonary arterial smooth muscle cells. MedChemComm *4*, 1394–1399.

Cancer Genome Atlas Research Network (2013). Comprehensive molecular characterization of clear cell renal cell carcinoma. Nature *499*, 43–49.

Chen, W., Hill, H., Christie, A., Kim, M.S., Holloman, E., Pavia-Jimenez, A., Homayoun, F., Ma, Y., Patel, N., Yell, P., et al. (2016). Targeting renal cell carcinoma with a HIF-2 antagonist. Nature *539*, 112–117.

Cho, H., Du, X., Rizzi, J.P., Liberzon, E., Chakraborty, A.A., Gao, W., Carvo, I., Signoretti, S., Bruick, R., Josey, J.A., et al. (2016). On-Target Efficacy of a HIF2alpha Antagonist in Preclinical Kidney Cancer Models. Nature *539*, 107–111.

Clifford, S.C., Cockman, M.E., Smallwood, A.C., Mole, D.R., Woodward, E.R., Maxwell, P.H., Ratcliffe, P.J., and Maher, E.R. (2001). Contrasting effects on HIF-1alpha regulation by disease-causing pVHL mutations correlate with patterns of tumourigenesis in von Hippel-Lindau disease. Hum. Mol. Genet. *10*, 1029–1038.

Cockman, M.E., Lippl, K., Tian, Y.M., Pegg, H.B., Figg, W.D.J., Jnr, Abboud, M.I., Heilig, R., Fischer, R., Myllyharju, J., Schofield, C.J., and Ratcliffe, P.J. (2019). Lack of activity of recombinant HIF prolyl hydroxylases (PHDs) on reported non-HIF substrates. eLife *8*, e46490.

Dobin, A., Davis, C.A., Schlesinger, F., Drenkow, J., Zaleski, C., Jha, S., Batut, P., Chaisson, M., and Gingeras, T.R. (2013). STAR: ultrafast universal RNA-seq aligner. Bioinformatics *29*, 15–21.

Gamper, A.M., Qiao, X., Kim, J., Zhang, L., DeSimone, M.C., Rathmell, W.K., and Wan, Y. (2012). Regulation of KLF4 turnover reveals an unexpected tissue-specific role of pVHL in tumorigenesis. Mol. Cell *45*, 233–243.

Godwin, J.L., Zibelman, M., Plimack, E.R., and Geynisman, D.M. (2014). Immune checkpoint blockade as a novel immunotherapeutic strategy for renal cell carcinoma: a review of clinical trials. Discov. Med. *18*, 341–350.

Gordeuk, V.R., Sergueeva, A.I., Miasnikova, G.Y., Okhotin, D., Voloshin, Y., Choyke, P.L., Butman, J.A., Jedlickova, K., Prchal, J.T., and Polyakova, L.A. (2004). Congenital disorder of oxygen sensing: association of the homozygous Chuvash polycythemia VHL mutation with thrombosis and vascular abnormalities but not tumors. Blood *103*, 3924–3932.

Haase, V.H. (2005). The VHL tumor suppressor in development and disease: functional studies in mice by conditional gene targeting. Semin. Cell Dev. Biol. *16*, 564–574.

Heinz, S., Benner, C., Spann, N., Bertolino, E., Lin, Y.C., Laslo, P., Cheng, J.X., Murre, C., Singh, H., and Glass, C.K. (2010). Simple combinations of lineage-determining transcription factors prime cis-regulatory elements required for macrophage and B cell identities. Mol. Cell *38*, 576–589.

Hoadley, K.A., Yau, C., Wolf, D.M., Cherniack, A.D., Tamborero, D., Ng, S., Leiserson, M.D.M., Niu, B.F., McLellan, M.D., Uzunangelov, V., et al. (2014). Multi-platform analysis of 12 cancer types reveals molecular classification within and across tissues-of-origin. Cell *158*, 929–944.

Hoffman, M.A., Ohh, M., Yang, H., Klco, J.M., Ivan, M., and Kaelin, W.G., Jr. (2001). von Hippel-Lindau protein mutants linked to type 2C VHL disease preserve the ability to downregulate HIF. Hum. Mol. Genet. *10*, 1019–1027.

Ivan, M., Kondo, K., Yang, H., Kim, W., Valiando, J., Ohh, M., Salic, A., Asara, J.M., Lane, W.S., and Kaelin, W.G., Jr. (2001). HIFalpha targeted for VHL-mediated destruction by proline hydroxylation: implications for O2 sensing. Science *292*, 464–468.

Jaakkola, P., Mole, D.R., Tian, Y.M., Wilson, M.I., Gielbert, J., Gaskell, S.J., von Kriegsheim, A., Hebestreit, H.F., Mukherji, M., Schofield, C.J., et al. (2001). Targeting of HIF-alpha to the von Hippel-Lindau ubiquitylation complex by O2-regulated prolyl hydroxylation. Science *292*, 468–472.

Kaelin, W.G., Jr. (2002). Molecular basis of the VHL hereditary cancer syndrome. Nat. Rev. Cancer *2*, 673–682.

Kondo, K., Klco, J., Nakamura, E., Lechpammer, M., and Kaelin, W.G., Jr. (2002). Inhibition of HIF is necessary for tumor suppression by the von Hippel-Lindau protein. Cancer Cell *1*, 237–246.

Kondo, K., Kim, W.Y., Lechpammer, M., and Kaelin, W.G., Jr. (2003). Inhibition of HIF2alpha is sufficient to suppress pVHL-defective tumor growth. PLoS Biol. *1*, E83.

Kunkel, G.T., Maceyka, M., Milstien, S., and Spiegel, S. (2013). Targeting the sphingosine-1-phosphate axis in cancer, inflammation and beyond. Nat. Rev. Drug Discov. *12*, 688–702.

Lee, D.C., Sohn, H.A., Park, Z.Y., Oh, S., Kang, Y.K., Lee, K.M., Kang, M., Jang, Y.J., Yang, S.J., Hong, Y.K., et al. (2015). A lactate-induced response to hypoxia. Cell *161*, 595–609.

Li, M., and Kim, W.Y. (2011). Two sides to every story: the HIF-dependent and HIF-independent functions of pVHL. J. Cell. Mol. Med. *15*, 187–195.

Li, L., Shen, C., Nakamura, E., Ando, K., Signoretti, S., Beroukhim, R., Cowley, G.S., Lizotte, P., Liberzon, E., Bair, S., et al. (2013). SQSTM1 is a pathogenic target of 5q copy number gains in kidney cancer. Cancer Cell *24*, 738–750.

Love, M.I., Huber, W., and Anders, S. (2014). Moderated estimation of fold change and dispersion for RNA-seq data with DESeq2. Genome Biol. *15*, 550.

Martin, M. (2011). Cutadapt removes adapter sequences from high-throughput sequencing reads. EMBnet.journal *17*, 10–12.

Nady, N., Krichevsky, L., Zhong, N., Duan, S., Tempel, W., Amaya, M.F., Ravichandran, M., and Arrowsmith, C.H. (2012). Histone recognition by human malignant brain tumor domains. J. Mol. Biol. *423*, 702–718.

Nam, Y., Sliz, P., Song, L., Aster, J.C., and Blacklow, S.C. (2006). Structural basis for cooperativity in recruitment of MAML coactivators to Notch transcription complexes. Cell *124*, 973–983.

Patro, R., Duggal, G., Love, M.I., Irizarry, R.A., and Kingsford, C. (2017a). Salmon provides fast and bias-aware quantification of transcript expression. Nat. Methods *14*, 417–419.

Patro, R., Duggal, G., Love, M.I., Irizarry, R.A., and Kingsford, C. (2017b). Salmon provides fast and bias-aware quantification of transcript expression. Nat. Methods *14*, 417–419.

Sauvageau, M., and Sauvageau, G. (2010). Polycomb group proteins: multi-faceted regulators of somatic stem cells and cancer. Cell Stem Cell *7*, 299–313.

Schnute, M.E., McReynolds, M.D., Kasten, T., Yates, M., Jerome, G., Rains, J.W., Hall, T., Chrencik, J., Kraus, M., Cronin, C.N., et al. (2012). Modulation of cellular S1P levels with a novel, potent and specific inhibitor of sphingosine kinase-1. Biochem. J. *444*, 79–88.

Semenza, G.L. (2012). Hypoxia-inducible factors in physiology and medicine. Cell *148*, 399–408.

Shlyueva, D., Stampfel, G., and Stark, A. (2014). Transcriptional enhancers: from properties to genome-wide predictions. Nat. Rev. Genet. *15*, 272–286.

Sjölund, J., Johansson, M., Manna, S., Norin, C., Pietras, A., Beckman, S., Nilsson, E., Ljungberg, B., and Axelson, H. (2008). Suppression of renal cell carcinoma growth by inhibition of Notch signaling in vitro and in vivo. J. Clin. Invest. *118*, 217–228.

Tang, M., Shen, H., Jin, Y., Lin, T., Cai, Q., Pinard, M.A., Biswas, S., Tran, Q., Li, G., Shenoy, A.K., et al. (2013). The malignant brain tumor (MBT) domain protein SFMBT1 is an integral histone reader subunit of the LSD1 demethylase complex for chromatin association and epithelial-to-mesenchymal transition. J. Biol. Chem. *288*, 27680–27691.

Tani, S., Kurooka, H., Aoki, T., Hashimoto, N., and Honjo, T. (2001). The N- and C-terminal regions of RBP-J interact with the ankyrin repeats of Notch1 RAMIC to activate transcription. Nucleic Acids Res. *29*, 1373–1380.

Wu, S., Trievel, R.C., and Rice, J.C. (2007). Human SFMBT is a transcriptional repressor protein that selectively binds the N-terminal tail of histone H3. FEBS Lett. *581*, 3289–3296.

Yang, H., Ivan, M., Min, J.H., Kim, W.Y., and Kaelin, W.G., Jr. (2004). Analysis of von Hippel-Lindau hereditary cancer syndrome: implications of oxygen sensing. Methods Enzymol. *381*, 320–335.

Yao, X., Tan, J., Lim, K.J., Koh, J., Ooi, W.F., Li, Z., Huang, D., Xing, M., Chan, Y.S., Qu, J.Z., et al. (2017). *VHL* Deficiency Drives Enhancer Activation of Oncogenes in Clear Cell Renal Cell Carcinoma. Cancer Discov. *7*, 1284–1305.

Zhang, J., and Zhang, Q. (2018). VHL and Hypoxia Signaling: Beyond HIF in Cancer. Biomedicines *6*, E35.

Zhang, Y., Liu, T., Meyer, C.A., Eeckhoute, J., Johnson, D.S., Bernstein, B.E., Nusbaum, C., Myers, R.M., Brown, M., Li, W., and Liu, X.S. (2008). Model-based analysis of ChIP-Seq (MACS). Genome Biol. *9*, R137.

Zhang, Q., Gu, J., Li, L., Liu, J., Luo, B., Cheung, H.W., Boehm, J.S., Ni, M., Geisen, C., Root, D.E., et al. (2009). Control of cyclin D1 and breast tumorigenesis by the EglN2 prolyl hydroxylase. Cancer Cell *16*, 413–424.

Zhang, J., Bonasio, R., Strino, F., Kluger, Y., Holloway, J.K., Modzelewski, A.J., Cohen, P.E., and Reinberg, D. (2013a). SFMBT1 functions with LSD1 to regulate expression of canonical histone genes and chromatin-related factors. Genes Dev. *27*, 749–766.

Zhang, J., Bonasio, R., Strino, F., Kluger, Y., Holloway, J.K., Modzelewski, A.J., Cohen, P.E., and Reinberg, D. (2013b). SFMBT1 functions with LSD1 to regulate expression of canonical histone genes and chromatin-related factors. Genes Dev. *27*, 749–766.

Zhang, L., Wang, X., Bullock, A.J., Callea, M., Shah, H., Song, J., Moreno, K., Visentin, B., Deutschman, D., Alsop, D.C., et al. (2015). Anti-S1P Antibody as a Novel Therapeutic Strategy for VEGFR TKI-Resistant Renal Cancer. Clin. Cancer Res. *21*, 1925–1934.

Zhang, J., Wu, T., Simon, J., Takada, M., Saito, R., Fan, C., Liu, X.D., Jonasch, E., Xie, L., Chen, X., et al. (2018). VHL substrate transcription factor ZHX2 as an oncogenic driver in clear cell renal cell carcinoma. Science *361*, 290–295.

STAR★METHODS

KEY RESOURCES TABLE

REAGENT or RESOURCE	SOURCE	IDENTIFIER
Antibodies		
Anti-SFMBT1	Bethyl	Cat # A303-221A; RRID:AB_10952224
Anti-HA Tag	Cell Signaling Technology	Cat # 3724S; RRID:AB_1549585
Anti-pVHL	Cell Signaling Technology	Cat # 68547S; RRID:AB_2716279
Anti-HIF1α	Cell Signaling Technology	Cat #14179; RRID:AB_2622225
Anti-OH-HIF1α	Cell Signaling Technology	Cat # D43B5; RRID:AB_2116958
Anti-FLAG-tag	Cell Signaling Technology	Cat #14793S; RRID:AB_2572291
Anti-SPHK1	Cell Signaling Technology	Cat #12071S; RRID:AB_2797815
Anti-Pan hydroxyproline	Abcam	Cat #ab37067; RRID:AB_873885
Anti-SFMBT1	Sigma-Aldrich	Cat #SAB1400557; RRID:AB_1856773
Anti-HIF2α	Abcam	Cat #ab157249
Anti-HIF1β	BD Biosciences	Cat #611078; RRID:AB_398391
Anti-Tubulin	Cell Signaling Technology	Cat #3873S; RRID:AB_1904178
Anti-ubiquitin	Santa Cruz Biotechnology	Cat # sc-8017; RRID:AB_2762364
Anti-biotin	Cell Signaling Technology	Cat # 5571s; RRID:AB_10892862
Anti-GST	Santa Cruz Biotechnology	Cat # sc-138; RRID:AB_627677
Bacterial and Virus Strains		
E. coli BL21	Homemade	N/A
Biological Samples		
Human ccRCC paired tissues	Tissue procurement facility at UNC	N/A
Chemicals, Peptides, and Recombinant Proteins		
Catalase	Millipore-Sigma	Cat #C-100
MG132	Peptide international	Cat #IZL-3175-v
DFO	Millipore-Sigma	Cat #D9533
FG4592	Millipore-Sigma	Cat #10338
DMOG	Frontier Scientific	Cat #D1070
Puromycin	GIBCO	Cat #A11138-03
Hygromycin	Invitrogen	Cat #10687010
PF543 Citrate	MedChem Express	Cat #HY-15425A
Biotin-HIF1 WT Peptide: DLDLEMLAPYIPMDDDFQLR	This paper	N/A
Biotin-HIF1 P564-OH: DLDLEMLAP#YIPMDDDFQLR	This paper	N/A
Biotin-SFMBT1 WT-OH: GKKKNKRIGRPPGGHSNLACA	This paper	N/A
Biotin-SFMBT1 P650-OH: GKKKNKRIGRP#PGGHSNLACA	This paper	N/A
Biotin-SFMBT1 P651-OH: GKKKNKRIGRPP#GGHSNLACA	This paper	N/A
Critical Commercial Assays		
Quick Change XL Site-Directed Mutagenesis Kit	Agilent Technologies	Cat #200516
Lipofectamine 3000 transfection reagent	Thermo Fisher Scientific	Cat #L3000015
TNT® Quick Coupled Transcription/Translation Systems	Promega	Cat #L1170
CellTiter 96 AQueous One Solution Cell Proliferation Assay	Promega	Cat #G3580

(*Continued on next page*)

Continued

REAGENT or RESOURCE	SOURCE	IDENTIFIER
Deposited Data		
Mendeley Database	This paper	GSE141577 https://doi.org/10.17632/zbx6x92dnv.1
Experimental Models: Cell Lines		
786-O	American Type Culture Collection	N/A
UMRC2	Sigmal	N/A
UMRC6	Sigmal	N/A
RCC4	Sigmal	N/A
HEK293T	American Type Culture Collection	N/A
HKC	From W. Kimryn Rathmell Lab	N/A
Experimental Models: Organisms/Strains		
NOD SCID Gamma mice	UNC Animal Studies Core	N/A
Recombinant DNA		
pCDNA-3.1-HA/FLAG-SFMBT1 (WT)	This paper	N/A
pGEX-4T1-VHL	This paper	N/A
pGEX-4T1-EglN1/2/3	This paper	N/A
pCDNA-3.1-HA-EglN1/2/3	This paper	N/A
pCDNA-3.1-HA-SFMBT1(P106A)	This paper	N/A
pCDNA-3.1-HA-SFMBT1(P651A)	This paper	N/A
plenti-UBCp-FLAG-HA-SFMBT1-gateway	This paper	N/A
plenti-UBCp-FLAG-HA-SFMBT1sh1-resistant-gateway	This paper	N/A
pll3.7-UBCP-EF1-SFMBT1	This paper	N/A
pll3.7-UBCP-EF1-SFMBT1(P651A)	This paper	N/A
pll3.7-UBCP-EF1-SFMBT1si1/3	This paper	N/A
pLX304-Blast-v5-SPHK1	UNC Lenti-shRNA Core Facility	N/A

LEAD CONTACT AND AVAILABILITY

Further information and requests for resources and reagents should be directed to and will be fulfilled by the Lead Contact, Qing Zhang (qing.zhang@utsouthwestern.edu).

All materials generated in this study are available from the Lead Contact with a completed Materials Transfer Agreement.

This study did not generate new unique reagents.

EXPERIMENTAL MODEL AND SUBJECT DETAILS

Orthotopic Tumor Growth

Six-week old NOD SCID Gamma mice (NSG, Jackson Lab) were used for xenograft studies. About 2×10^6 viable 786-O kidney cancer cells were resuspended in 20 μL fresh growth medium and injected orthotopically into the left kidney of each mouse as described previously (Li et al., 2013). Bioluminescence imaging was performed as described previously (Zhang et al., 2009), after making sure tumors were successfully implanted in the kidney, mice were fed Purina rodent chow with doxycycline (#5001, Research Diets Inc.). Mice were euthanized 7 weeks after treatment with doxycycline. All animal experiments were in compliance with National Institutes of Health guidelines and were approved by the University of North Carolina at Chapel Hill Animal Care and Use Committee.

METHOD DETAILS

Genome-Wide Screening

A cDNA library containing approximately 17,000 human ORFs was purchased from Mammalian Gene Collection (MGC). These ORF clones were purchased as bacterial stock in a 96-well plate format. To convert the library into plasmid DNA for *in vitro* protein synthesis, the bacterial stock for each ORF clone was cultured separately in LB media overnight, the density of the cultures was measured the next morning and equal amounts of bacteria was taken from the cultures of 24 different clones and mixed together for miniprep (QIAGEN). Eluted plasmid DNA for each pool of 24 clones was arranged in a 96-well plate (Ayad et al., 2005). Through

this approach, the whole library was converted to about 700 pools of plasmid DNA with 24 individual clones/pool. For *in vitro* protein synthesis, 1 μL of each DNA pool was added to 4 μL of *in vitro* transcription/translation (IVT) master mix (Promega) in the presence of ^{35}S Methionine. The IVT mixtures were incubated at 37°C for 90 min for the production of *in vitro* translated proteins. Upon completion of IVT, 2 μL of each IVT mixture was incubated with GST-VHL complex (containing GST-VHL, Elongin B and C mixture) bound to glutathione beads (Yang et al., 2004) with either WT HIF1α peptide or hydroxylated HIF1α peptide as a competitor for 4 h. Subsequently, the reaction mixtures were washed 4 times with NETN lysis buffer, and proteins bound to the glutathione beads were eluted and resolved on an SDS-PAGE. Finally the protein gels were dried for auto-radiography.

In vitro decarboxylation assay

In brief, peptides were supplemented with 50 mM HEPES (pH 7.4), 1500 U/mL catalase, 100 mM $FeSO_4$, 1 mM ascorbic acid, 0.15 μCi/mL [1-^{14}C] α-KG (Perkin Elmer), and 2 μg of recombinant EglN1 enzyme (Active motif, 81765) in a 100 μL reaction volume. Radiolabeled CO_2 was captured with glass fiber filter paper (catalog no. IH-201-A, Inotech Biosystems International).The reaction was quenched by KH_2PO_4 buffer. The reaction mixture was transferred to a 37°C oven and allowed to incubate for 1 h and then shaken for 30 min at room temperature. The CPM value was determined using a liquid scintillation analyzer (PerkinElmer).

Human ccRCC paired tissues

For human ccRCC paired tissues, fresh-frozen samples of ccRCC and adjacent normal tissues were obtained from the tissue procurement facility at UNC. Tissues were diced, lysed in 8M Urea buffer and followed by sonication. The lysates were subjected to western blotting as described above. IRB approval (13-1986 from UNC Chapel Hill) was obtained before obtaining these human tumor and normal tissues.

IHC and TMA

For IHC and TMA with SFMBT1 and SPHK1, a rabbit polyclonal antibody against SFMBT1 was purchased from Atlas Antibodies (HPA064564). A rabbit polyclonal antibody against SPHK1 was purchased from Cell Signaling (D1H1). IHC was carried out in the Bond Autostainer (Leica Microsystems Inc.; Norwell MA). Briefly, slides were dewaxed in Bond Dewax solution (AR9222) and hydrated in Bond Wash solution (AR9590). Antigen retrieval was performed for 20 min at 100°C in Bond-Epitope Retrieval solution 1, pH-6.0 (AR9961). Slides were incubated with primary antibody (1:150) for 30min (SFMBT1), and then with second antibody (Leica, RE7261). Antibody detection was performed using the Bond Intense R detection system (DS9263) with ImmPress HRP anti-rabbit IgG (MP-7451; Vector Laboratories; Burlingame, CA). Stained slides were dehydrated and coverslipped. Positive and negative controls (no primary antibody) were included during the run. For digital imaging and image analysis, stained slides were digitally scanned at 20x magnification using Aperio ScanScope-XT (Aperio Technologies, Vista, CA) were uploaded to the Aperio eSlideManager database (Leica Biosystems Inc; eSlideManager version 12.3.3.7075) at the Translational Pathology Laboratory at UNC. TMA images were digitally segmented into cores using TMALab (Aperio). Individual TMA cores were separately analyzed using the Aperio Cytoplasmic v2 algorithm with slight adjustments for cell shape. The number and percentage of cells with light (1+), medium (2+) and strong (3+) nuclei and/or cytoplasmic staining was determined. H Scores were calculated using the following formula: 3 x percentage of strongly staining nuclei + 2 x percentage of moderately staining nuclei + percentage of weakly staining nuclei, giving a range of 0 to 300.

LC-MS/MS analysis

Cell lysate from FLAG-SFMBT1 expressing cells treated with either MG132 or MG132 together with DMOG was immunoprecipitated from 293T cells. Immunoprecipitates were separated by SDS-PAGE and visualized by Coomassie staining. Bands corresponding to SFMBT1 were excised and the proteins were reduced, alkylated and digested with trypsin overnight at 37°C followed by mass spectrometry. Peptides were extracted, desalted with C18 spin columns (Pierce) then dried via vacuum centrifugation.

Transfection, Virus Production and Infection

For immunoprecipitation, 1.5 × 10^6 293T cells were treated with drugs for 8 h or overnight and lysates were harvested 48 h post transfection (hpt). Lentiviruses were prepared by transfecting 293T cells (2 × 10^6 cells in 100-mm dishes) as previously described (Zhang et al., 2009). Following a media change at 12 hpt, the supernatant containing the lentiviruses were harvested at 48 and 72 hpt. After filtering with 0.45-μm filters, viruses were used to infect target cells in the presence of polybrene (8 μg/mL) or stored at −80°C.

Cell Proliferation Assays and Anchorage-Independent Growth assay

For cell proliferation assays, cells were seeded in triplicate in 96-well plates (1000 cells/well) in appropriate growth medium. 10000 cells/mL for 786-O cells and 3000 cells/mL for UMRC2 were used in anchorage-independent growth assay as described previously (Zhang et al., 2018).

Immunoprecipitation and GST pull-down assay

For the protein immunoprecipitation assay (IP), the cell pellets were lysed in EBC buffer for 30 min. After sonication, cells were spun at 12,000 g for 5 min at 4°C to remove debris. 1 μg protein from whole cell lysate was incubated with indicated antibodies or anti-FLAG

M2 affinity gel (Sigma-Aldrich, A2220) / 3F10 HA conjugated beads (Roche Applied Bioscience, 11815016001) overnight or 4 h at 4°C. Lysate incubated with antibodies was added to 10 μL of protein G agarose beads (Roche Applied Bioscience, 11243233001) with rotation for an additional 3 h at 4°C.

For the binding between FLAG-VHL and HIF1α and SFMBT1 peptides, Comparable amounts of Biotin-tagged HIF1α (WT and P564-OH) or SFMBT1 (WT, P650-OH and P651-OH) peptides were incubated with NeutrAvidin Agarose Resin (Thermo, 29200) for 4 h at 4°C. Mixtures were centrifuged, washed with EBC buffer and then mixed with *in vitro* translated (IVT) Flag-VHL overnight at 4°C. The bound complexes were then centrifuged, washed with EBC buffer, subjected to SDS-PAGE, and immunoblotted with FLAG antibody.

For the GST pull-down assay, IVT protein or protein from whole cell lysates were incubated with indicated GST fusion proteins overnight or 4 h at 4°C. Bound complexes were centrifuged, washed with EBC buffer, subjected to SDS-PAGE, and immunoblotted for the indicated targets.

Ubiquitination assay

Cells were harvested and extracted in 100 μL of EBC buffer containing 1% SDS. Cell extracts were heat-denatured for 5 min at 95°C and diluted with 900 μL EBC buffer. After sonication and centrifugation, cell lysates were subjected to immunoprecipitation with ubiquitin antibody (Santa Cruz Biotechnology, sc-8017).

In vitro hydroxylation followed by VHL binding assay

Comparable amounts of Biotin-tagged HIF1α or SFMBT1 peptides were mixed with reaction buffer (50 mM HEPES, 1500 U/mL catalase, 100 μM FeSO4, 5 mM ascorbic acid, 1 mM α-KG) and IVT HA-EglN1, IVT HA-EglN1-CD protein (enzyme) or negative control buffer (150 mM NaCl, 5 μM FeSO4, 50 mM Tris-HCl, pH 7.5). The reaction mixture was incubated at 37°C for 1 h.

The reaction mixture was then incubated with NeutrAvidin™ Agrose Resin for 3-5 h, washed by EBC buffer and incubated with IVT FLAG-pVHL overnight at 4°C. Agrose Resin was collected by centrifugation, washed with EBC and subjected to immunoblot with an anti-FLAG antibody.

QUANTIFICATION AND STATISTICAL ANALYSIS

RNA-Seq analysis

RNA was extracted from 786-O cells using RNeasy kit with on-column DNase digestion (QIAGEN), and sequenced at BGI as single-end 50 bp reads. Reads were then filtered for adaptor contamination using cutadapt (Martin, 2011) and filtered such that at least 90% of bases of each read had a quality score > 20. Reads were aligned to the reference genome (hg19) using STAR version 2.5.2b retaining only primary alignments (Dobin et al., 2013). Reads overlapping blacklisted regions of the genome were then removed. Transcript abundance was then estimated using salmon (Patro et al., 2017b), and differential expression was detected using DESeq2 (Love et al., 2014). HIF2α RNA Seq data was obtained from GSE86095 (Yao et al., 2017).

TCGA data

TCGA provides a kidney renal clear cell cancer (KIRC) dataset which was previously processed and described (Hoadley et al., 2014). For mRNA expression data, we used RNA-seq by STAR-Salmon (Patro et al., 2017a) to quantify the transcript abundances measured by RNA sequencing and used the log2-transformed up-quantile-normalized (Bullard et al., 2010) STAR-Salmon values of the genes. We compared these gene expression between *VHL* WT and *VHL* mutant patients, by two-class unpaired t test. We compared these gene expression between Stage I, II, III, IV and normal patients by Analysis of Variance (ANOVA).

Chromatin immunoprecipitation and Integrated analysis

ChIP was performed with SFMBT1 antibody (Bethyl, A303-221A) as previously described (Zhang et al., 2018). ChIP-seq libraries (Illumina) were prepared according to manufacturer's recommendations and sequenced at the UNC High Throughput Genomic Sequencing facility using single-end 50bp reads. Reads were then filtered for adaptor contamination using cutadapt (Martin, 2011) and filtered such that at least 90% of bases of each read had a quality score > 20. Duplicated sequences were then capped at a maximum of 5 occurrences, and reads were aligned to the reference genome (hg19) using STAR (Dobin et al., 2013) version 2.5.2b retaining only primary alignments. Reads overlapping blacklisted regions of the genome were then removed. Reads were then extended *in silico* to a fragment size of 250 bp, and regions of significant enrichment relative to input control were identified using MACS2 (Zhang et al., 2008). Motifs were identified by comparing the 200 bp surrounding the peak midpoint to the 200 bp flanking sequence on either side of each identified peak using HOMER (Heinz et al., 2010). HIF ChIP-seq data were obtained from GSE34871, and histone modification ChIP-seq were obtained from GSE86095. Selection of important SFMBT1 direct target genes in ccRCC was based on the following criteria: For TCGA ccRCC data, Cox P value < 0.05, C-index > 0.5 and Cox hazard ratio is above 1; Tumor-normal t test P value < 0.05 and Tumor-normal Log_2FC value > 0.1. In addition, these genes should have SFMBT1, H3K4me3 and H3K27ac binding peaks in promoter regions.

Statistical analysis

The unpaired two-tail Student's t test was used for experiments comparing two sets of data, unless otherwise indicated. For quantification of cell proliferation assays, if there were multiple comparisons with multiple time points and comparison groups, we multiplied the raw p values by the number of comparisons (number of time points x number of experimental groups, in each plot) to get Bonferroni adjusted p values for each comparison (in each plot). The significance of comparisons were then based in adjusted p values. Mann-Whitney tests were used for animal experiments. Data represent mean ± SD from at least three independent experiments.

DATA AND CODE AVAILABILITY

All data generated or analyzed during this study are included in Figures 1-7 and Figures S1–S7. Additional datasets that support the findings of this study are available from the corresponding author upon reasonable request. ChIP-seq and RNA-seq data have been deposited to GEO under accession number GSE141577.